

Estimation of actual evapotranspiration from remote sensing: application in a semiarid region

García Galiano S.G., García Cárdenas R.

in

Erena M. (coord.), López-Francos A. (coord.), Montesinos S. (coord.), Berthoumieu J.-P. (coord.).

The use of remote sensing and geographic information systems for irrigation management in Southwest Europe

Zaragoza : CIHEAM / IMIDA / SUDOE Interreg IVB (EU-ERDF)
Options Méditerranéennes : Série B. Etudes et Recherches; n. 67

2012
pages 105-117

Article available on line / Article disponible en ligne à l'adresse :

<http://om.ciheam.org/article.php?IDPDF=00006601>

To cite this article / Pour citer cet article

García Galiano S.G., García Cárdenas R. **Estimation of actual evapotranspiration from remote sensing: application in a semiarid region.** In : Erena M. (coord.), López-Francos A. (coord.), Montesinos S. (coord.), Berthoumieu J.-P. (coord.). *The use of remote sensing and geographic information systems for irrigation management in Southwest Europe.* Zaragoza : CIHEAM / IMIDA / SUDOE Interreg IVB (EU-ERDF), 2012. p. 105-117 (Options Méditerranéennes : Série B. Etudes et Recherches; n. 67)



<http://www.ciheam.org/>
<http://om.ciheam.org/>

Estimation of actual evapotranspiration from remote sensing: Application in a semiarid region

S.G. García Galiano and R. García Cárdenas

Universidad Politécnica de Cartagena, Department of Civil Engineering,
R&D Group of Water Resources Management, Paseo Alfonso XIII, 52, 30203, Cartagena (Spain)

Abstract. The potential of remote sensing for the recommendation and monitoring of irrigation practices is irrefutable. GIS have enabled the development of operational spatio-temporal tools for monitoring agricultural activity which can overcome the uncertainty brought about by problems related to water scarcity and increasing drought events. This paper presents an operational methodology for estimating actual evapotranspiration from Landsat images, and its application in the Region of Murcia (Spain).

Keywords. Remote sensing – GIS – Actual evapotranspiration – Land surface temperature – NDVI.

Estimation de l'évapotranspiration réelle à partir de la télédétection : application dans une région semi-aride

Résumé. Le potentiel que représente la télédétection pour la recommandation et le suivi des pratiques d'irrigation est irréfutable. Couplées avec un SIG, les images de télédétection permettent le développement d'outils opérationnels spatio-temporels utiles pour le suivi des activités agricoles. Ce papier présente une méthodologie opérationnelle pour l'estimation de l'évapotranspiration réelle à partir d'images Landsat et son application dans la Région de Murcia (Espagne).

Mots-clés. Télédétection – GIS – Evapotranspiration réelle – Température de surface des terres – NDVI.

I – Introduction

The potential of remote sensing for the recommendation and monitoring of irrigation practices is irrefutable. The context of uncertainty in the rural areas of the southwest Mediterranean area, especially in agriculture, is caused by the loss of competitiveness and abandonment of farming in many areas due to problems related to water scarcity and the increase of drought events.

The Southeastern Spanish basins are regularly affected by drought. These events affect large areas, and their severity has increased in recent years due to climate change (García Galiano *et al.*, 2011). This situation endangers the continuity of significant areas of irrigation, critical in this case for the economy of the Region of Murcia. Moreover, the adjusted water allocations for irrigation in the region, coupled with quality problems that necessarily arise from the intensive use of resources, will continue setting up a situation of scarcity. It is conceivable that repeated acute episodes of lack of water for irrigation, such as those registered in recent years, will have to be faced in the coming decades with greater intensity.

As a result, the assessment and monitoring of irrigated areas presents special relevance. Remote sensing has proved to be a very efficient tool for this, allowing the estimation of vegetation indices related to the soil water content and actual evapotranspiration directly. The present study addresses the operational development in a GIS (Geographical Information System) environment, a remote sensing based methodology for estimating actual evapotranspiration and its application in the Region of Murcia.

II – Target zone and databases

1. Segura River Basin and its level of spatial disaggregation

The study area corresponds to the Segura River Basin (SRB, Spain), located in the southeastern part of the Iberian Peninsula (Fig. 1). The semiarid SRB, with an area of 18,870 km², presents the lowest percentage of renewable water resources of all Spanish basins and it is currently highly regulated.

The main water demand is agriculture, with a surface of more than 43% (809,045 ha) of the basin (SRBP, 1998), with one third of that surface being under irrigation (269,000 ha). Agricultural water demand from irrigated areas must be highlighted because it accounted for 85% of the total water demand in 2007 (Urrea *et al.*, 2011).

In addition, available water resources per inhabitant in the Segura River Basin (only 442 m³/inhabitant/year) are much lower than the national water scarcity threshold, which is set at 1000 m³/inhabitant/year, according to the United Nations and the World Health Organization. Water scarcity is a major issue in the Segura River Basin. Consequently, water transfer from the Tajo River Basin, supplemented with desalinization, are real options for increasing water resources in the basin.

The SRB is controlled by head water reservoirs, where natural runoff is regulated, and by reservoirs that store the water resources from the Tajo River Basin. With the aims of planning and managing water resources, and considering the specificities of the basin, several levels of spatial disaggregation are identified: hydraulic zones, systems of exploitation of resources, and units of exploitation. The evaluation of resources and demands and possibilities of management, considering the hydraulic infrastructures of the basin, are analyzed from the disaggregation into hydraulic zones and sub-zones according to the Segura River Basin Management Plan (SRBP, 1998). The hydraulic zones (Fig. 1) were defined considering topographical criteria (basins and sub-basins) and administrative limits. There are fourteen hydraulic zones in the SRB.

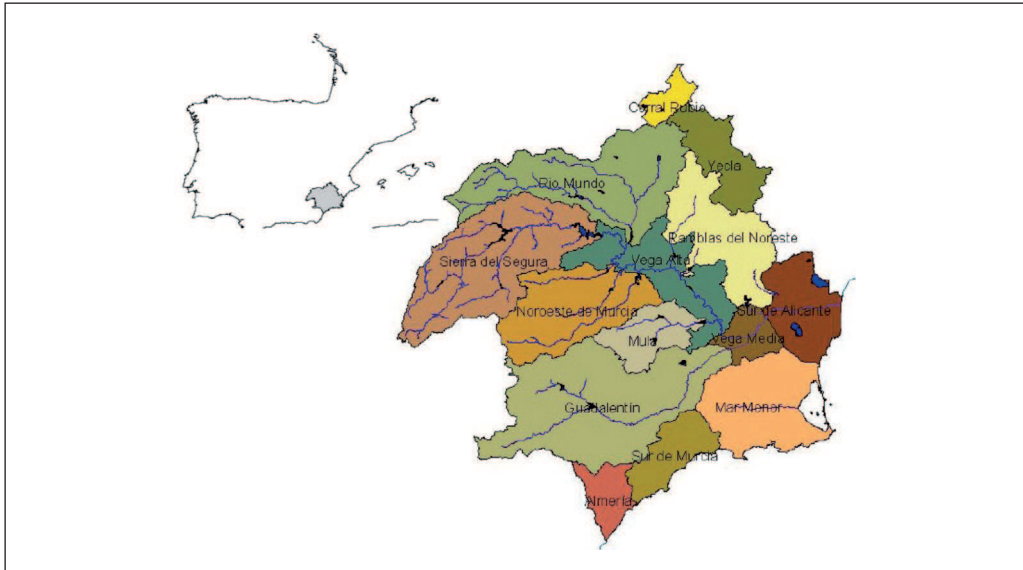


Fig. 1. Location of the Segura River Basin, and hydraulic zones (Source: Hydrographic Confederation of Segura River Basin (CHS), Ministry of Environment, Marine and Rural Affairs).

Based on these hydraulic zones, the CHS defined several Systems of Exploitation of Resources (SER). These SER are further aggregated in the frame of the Segura River Basin Drought Action Plan (SRBDAP, 2007).

Finally, considering the water demands and sources, several spatial disaggregation schemes could be identified for the basin, each one corresponding to specific objectives. For example, the Spanish Institute of Statistics (INE) identifies *agricultural areas* (Fig. 2). In turn, these areas can be identified as rain fed or *irrigated-zones*, and the latter can be further identified into irrigated zones using the Basin System resources or the water supplied by ATS. The CHS in turn, consider the use of UDAs (Units of Agriculture Demands).

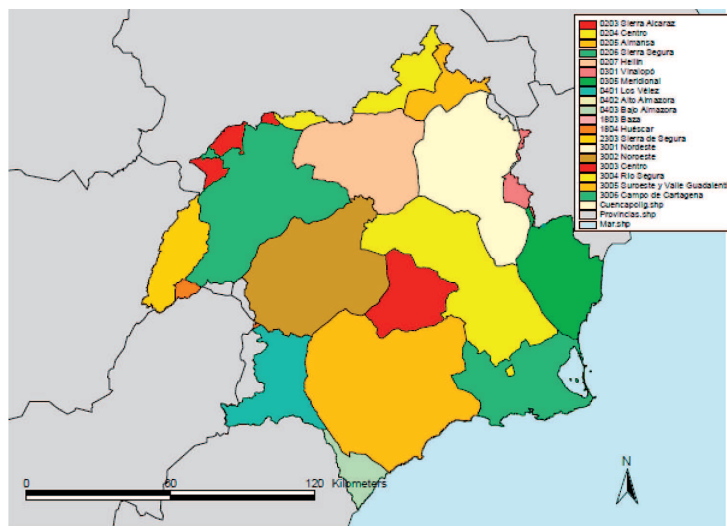


Fig. 2. Spatial disaggregation of agricultural zones [Source: National Institute of Statistics (INE, Spain)].

2. Datasets: Collection of spatio-temporal information

Several sources of information were considered: the National Plan of Remote Sensing (PNT), the CHS water agency, the Instituto Murciano de Investigación Agraria y Alimentaria (IMIDA), as well as information freely accessible on the Internet.

The satellite data used corresponded to Landsat 5 TM (TM5), Spot 5, and MODIS data. However, the work was mainly based on Landsat 5 TM and MODIS data. The MODIS (Moderate Resolution Imaging Spectroradiometer) is a sensor, on the TERRA (EOS AM) and AQUA (EOS PM) platforms of NASA.

The Landsat images cover a total surface of 185x185 km². These images were geometrically rectified, and georeferenced considering the ETRS-89 system with UTM projection by the Instituto Geográfico Nacional (IGN).

For considering the whole SRB in a specified date, the acquisition of the following four images are needed: 199-33, 199-34, 200-33, and 200-34 (Fig. 3). A time lag between 199-33/199-34 and 200-33/200-34 will be identified. Therefore, it is not possible to study the whole basin for the same date. The Region of Murcia is included in the spatial framework of 199-33 and 199-34 images.

NDVI was derived from reflectance values in the Red (B3) and infrared (B4) region of the electromagnetic spectrum of TM5 images, as follows:

$$NDVI = (B4 - B3) / (B4 + B3) \quad (1)$$

The range of NDVI correspond from -1 to 1, but for this study the range 0 (bare soil) to 1 (soil with maximum plant biomass), was considered. Then, negative values represent water. Fig. 5 shows the spatial distribution of NDVI for two dates (14/02 and 24/07 of 2009), in the Region of Murcia.

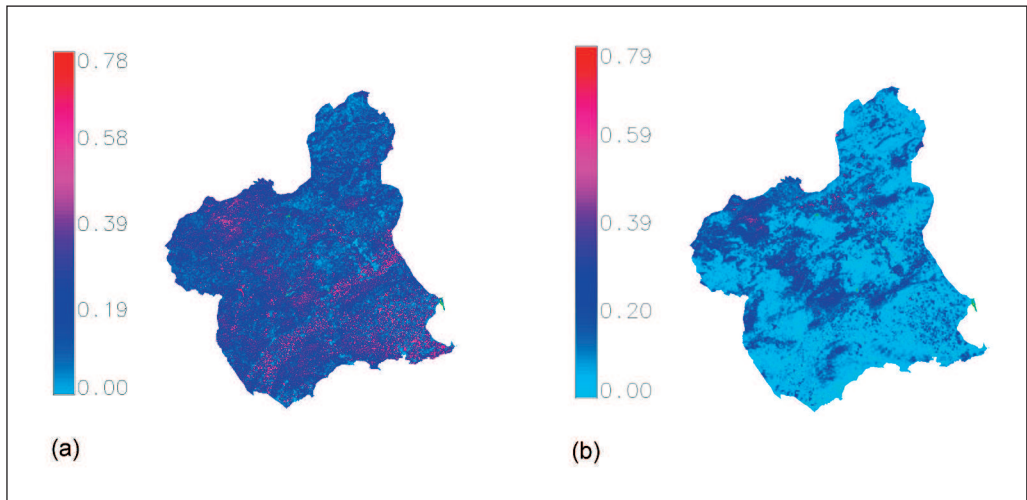


Fig. 5. Spatial distribution of NDVI for the Region of Murcia, from TM5: (a) 14/02/2009 and (b) 24/07/2009.

2. Estimation of time evolution of LST

The LST was estimated from band 6 of Landsat, with spatial resolution of 120 m. The LST spatial distribution in combination with vegetation indexes will be considered in the estimation of indicators related with soil moisture (Sandholt *et al.*, 2002) and actual evapotranspiration (Jiang and Islam, 2001). The LST spatial distributions from TM5 were contrasted with the LST product provided by MODIS sensor. SPOT images do not present thermal band.

In the following paragraphs, the methodology for the estimation of LST from Landsat is presented. The geometric correction was not needed for Landsat images, because they correspond to PNT, and the corrections were already made. The signals received by the thermal sensors (TM5) can be converted to at-sensor radiance (L_{sensor}), according to the corrections proposed by Voogt and Oke (2003):

- (i) Spectral radiance conversion to at-sensor brightness temperature,
- (ii) Correction by atmospheric absorption and re-emission,
- (iii) Correction by surface emissivity, and
- (iv) Correction by surface roughness.

In the case of correction (i), the signal received from the thermal sensor could be converted to different parameters for the LST estimation,

$$L_{sensor} = gain.DN + bias \quad (2)$$

where L_{sensor} is the spectral radiance of thermal band, DN is the digital number of a given pixel (in this case, each pixel of TM5 band 6), $gain$ is the slope of the radiance/ DN conversion function depending of the band (for band 6, the $gain$ is 0.055158), and $bias$ is the intercept of the radiance/ DN conversion function; it is a constant depending on the band ($bias=1.238$ for TM5 band 6)

$$T_{sensor} = \frac{K_2}{\ln\left(\frac{K_1}{L_{sensor}} + 1\right)} \quad (3)$$

where T_{sensor} represents the at-sensor brightness temperature (K) with $K_1 = 607.76 \text{ W}/(\text{m}^2\text{sr}\cdot\mu\text{m})$ and $K_2 = 1260.56 \text{ K}$ as prelaunch calibration constants for TM5 (Landsat Project Science Office, 2002), and L_{sensor} estimated above.

To obtain LST, the following steps correspond to correction (ii) to (iv), the single-channel algorithm proposed by Jiménez-Muñoz and Sobrino (2003) must be applied.

$$T_s = \gamma \left[\varepsilon^{-1} (\psi_1 L_{sensor} + \psi_2) + \psi_3 \right] + \delta \quad (4)$$

with

$$\gamma = \left\{ \frac{c^2 L_{sensor}}{T_{sensor}^2} \left[\frac{\lambda^4}{c_1} L_{sensor} + \lambda^{-1} \right] \right\}^{-1} \quad (5)$$

$$\delta = -\gamma L_{sensor} + T_{sensor} \quad (6)$$

where T_s is the LST in K, ε is the ground surface emissivity, $c_1 = 1.19104 \cdot 10^8 \text{ (W } \mu\text{m}^4\text{m}^{-2}\text{sr}^{-1})$, and $c^2 = 14387.7 \text{ (}\mu\text{m K)}$, λ is the effective wave length (μm) corresponding to band 6.

The following equations represent the correction by total atmospheric water vapour content (w in grs/cm^2), therefore the atmospheric functions (ψ_1 , ψ_2 and ψ_3) depend only on w , particularized for TM/ETM+ 6 data, as follows,

$$\begin{aligned} \psi_1 &= 0.14714w^2 - 0.15583w + 1.1234 \\ \psi_2 &= -1.1836w^2 - 0.37607w - 0.52894 \\ \psi_3 &= -0.04554w^2 + 1.8719w - 0.39071 \end{aligned} \quad (7)$$

For the estimation of atmospheric water vapour, external data are needed. In this case, the MODIS Terra Level 2 Water Vapour product MOD05_L2 (Gao and Kaufman, 1998), could be used because the hour the satellite passes over the Iberian Peninsula is similar to Landsat. But the MODIS data are available from 2000, therefore for previous years the AVHRR sensor of NOAA satellite could be considered.

However, in the present work the maps of water vapour (grs/cm^2) were generated from monthly values provided for typical clear days by the SoDA Project (<http://www.soda-is.com>) stations in different parts of the Region of Murcia, according to Remund *et al.* (2003).

The last step for the estimation of LST from Landsat is the calculation of the surface emissivity (ε). The ε values could be obtained for example based on classification image, based on NDVI

image or based on the ratio values of vegetation and bare ground (Zhang *et al.*, 2006). In this work, the ϵ values are estimated in function of NDVI (Valor and Caselles, 1996) as follows,

$$\begin{aligned}
 -1 < \text{NDVI} < -0.18 \quad \epsilon &= 0.985 \\
 -0.18 < \text{NDVI} < 0.157 \quad \epsilon &= 0.955 \\
 0.157 < \text{NDVI} < 0.727 \quad \epsilon &= 1.0094 + 0.047 \ln(\text{NDVI}) \\
 0.727 < \text{NDVI} < 1 \quad \epsilon &= 0.99
 \end{aligned}
 \tag{8}$$

Fig. 6 presents an example of the application of the methodology described in the estimation of LST for Murcia Region (date 24/07/2009).

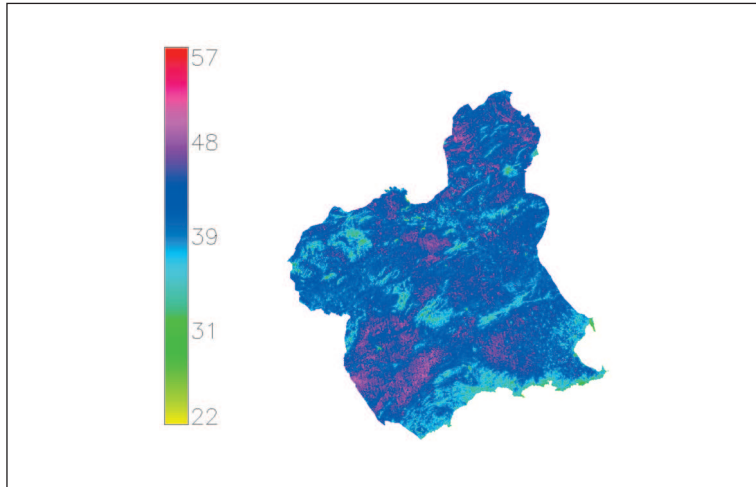


Fig. 6. Spatial distribution of LST (°C) for date 24/07/2009 (LSTD20090724).

The results of NDVI and LST derived from TM5 could be compared with the corresponding products from MODIS TERRA. In this case, the product MOD11A1 (daily LST with spatial resolution 1x1 km) and product MOD09GA (daily reflectances with spatial resolution 500x500 m), could be used. From MOD09GA the NDVI is estimated, combining bands 1 and 2, as $NDVI = (B2 - B1) / (B2 + B1)$. From the comparison of images, the differences detected are neglectable.

IV – Application of JIC Algorithm derived from the residual method

An algorithm derived from the *residual method*, proposed by Jiang *et al.* (2004) or the JIC method, was selected. In the JIC method, the ET_{act} is based on the direct estimation of the evaporative fraction (EF), without estimation of H_s , as follows

$$\lambda ET = \phi \frac{\Delta}{(\Delta + \gamma)} (R_N - G)
 \tag{9}$$

where ϕ is the evaporative fraction (EF), Δ is the slope of the vapour pressure, γ the psychrometric constant, R_N is the net radiation, and G is the flux of soil heat.

This method requires a prior graphical representation and interpretation of LST-NDVI space. This space (triangular or trapezoidal in form), delimited by the distribution of pixels, has a linear relationship with the surface fluxes of energy. Each pixel of the space presents a specific Φ defined by,

$$\phi = \phi_{\max} \frac{LST_{\max} - LST}{LST_{\max} - LST_{\min}} \quad (10)$$

where $\Phi_{\max} = 1.26$ corresponds to bare soil, LST_{\max} is the maximum LST for NDVI = 0, and LST_{\min} the minimum LST. Then, a spatial distribution of Φ is obtained for each date.

The following equation represents the evaporative fraction (EF),

$$EF = \phi \frac{\Delta}{(\Delta + \gamma)} \quad (11)$$

where the psychrometric constant is a function of atmospheric pressure by the following equation,

$$\gamma = 0.665 \cdot 10^{-3} P \quad (12)$$

where P is the atmospheric pressure (kPa), depending on height (on normal climatology conditions), as:

$$P = P_0 e^{\left(\frac{-z}{8000}\right)} \quad (13)$$

where z is the height in meters above sea level, and P_0 atmospheric pressure (kPa) at sea level.

The Δ is the slope of the vapour pressure, is estimated as follows,

$$\Delta = \frac{4098 \cdot 0.6108}{(T_a + 237.3)^2} \exp\left(\frac{17.27 T_a}{T_a + 237.3}\right) \quad (14)$$

The maps of relative humidity (HR) and air temperature are obtained from meteorological stations. Fig. 7, presents an example of HR and T_a maps, for the date 24/07/2009. From these maps, the spatial distributions of e^* (saturated vapour pressure) and e_a (air vapour pressure), were derived.

The saturated vapour pressure (e^*) could be estimated only depending on surface temperature (LST), and, finally the e_a is estimated from HR (%) and e^* , as follows,

$$e_a = \frac{HR e^*}{100} \quad (15)$$

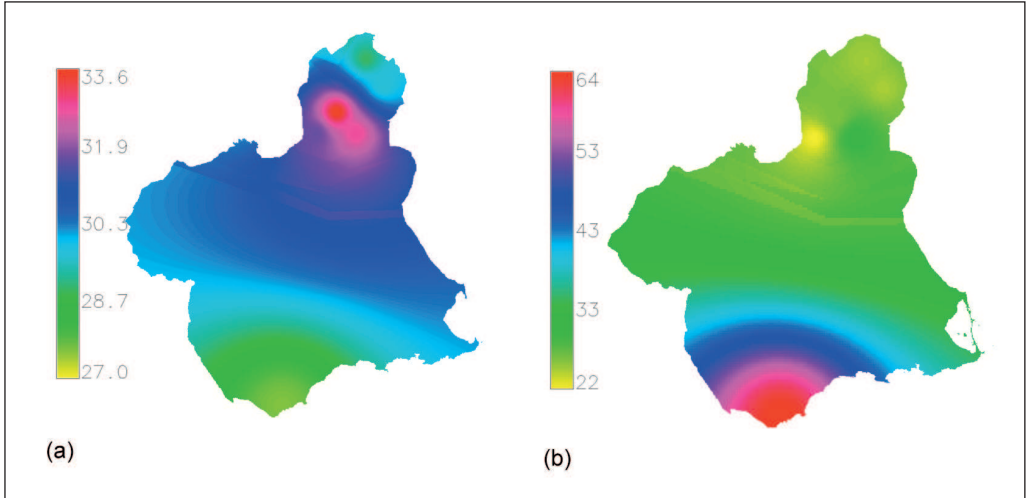


Fig. 7. Mean daily spatial distribution for the Region of Murcia: (a) T_a (°C), and (b) HR.

V – Estimation of net radiation

The net radiation (R_N , $\text{Wm}^{-2}\text{day}^{-1}$) is estimated considering ground meteorological data, remote sensing data, and topographical attributes derived from a Digital Elevation Model (DEM), applying the following equation,

$$R_N = R_s^\downarrow + R_s^\uparrow + R_L^\downarrow + R_L^\uparrow = (1 - \alpha)R_s^\downarrow + R_L^\downarrow + R_L^\uparrow \quad (16)$$

where R_s^\downarrow and R_s^\uparrow are downward and upward shortwave solar global radiation, respectively, R_L^\downarrow and R_L^\uparrow are downward and upward long wave radiation, respectively. They were estimated considering the Stefan Law, with the clear sky emissivity calculated from an empirical relationship with e_a , and the surface emissivity.

1. Estimation of ($R_s^\downarrow + R_s^\uparrow$) shortwave net radiation

The diffuse, direct (beam) and ground reflected solar irradiation for given day, latitude, surface and atmospheric conditions, could be estimated for clear-sky and overcast atmospheric conditions with the *r.sun* model below GRASS GIS (GRASS, 2011). Therefore, the term ($R_s^\downarrow + R_s^\uparrow$) or net balance of shortwave global radiation is derived from the results of the *r.sun* command.

The *r.sun* model considers all relevant input parameters as spatially distributed entities to enable computations for large areas with complex terrain (Šúri and Hofierka, 2004). Conceptually, the model is based on equations of European Solar Radiation Atlas (ESRA). As an option, the model considers a shadowing effect of the local topography. The *r.sun* works in two modes. In the first mode it calculates a solar incidence angle (degrees) and solar irradiance values (Wm^{-2}) for the set local time. In the second mode, used in the present work, daily sums of solar radiation ($\text{Whm}^{-2}\text{day}^{-1}$) are computed within a set day.

The input data correspond to:

- A DEM (meters) and topographical attributes such as slope and aspect (both in decimal degrees), are used. In this case, a DEM with a spatial resolution of 30 m was considered. The

topographical attributes were derived from the DEM, applying the GRASS GIS command *r.slope.aspect*. Fig. 8, below, presents the DEM and aspect maps for the Region of Murcia.

- Latitude map (decimal degrees, from -90° to 90°), is the other map required.

Then, the spatial distribution of slope and latitude are presented in Fig. 9.

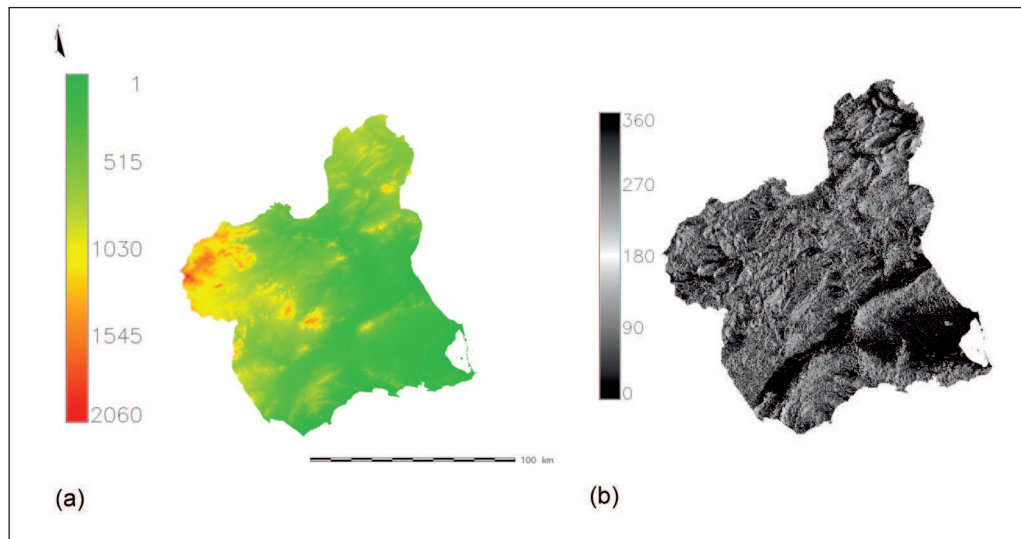


Fig. 8. Spatial distributions for the Region of Murcia: (a) DEM (m), and (b) aspect (grades from East).

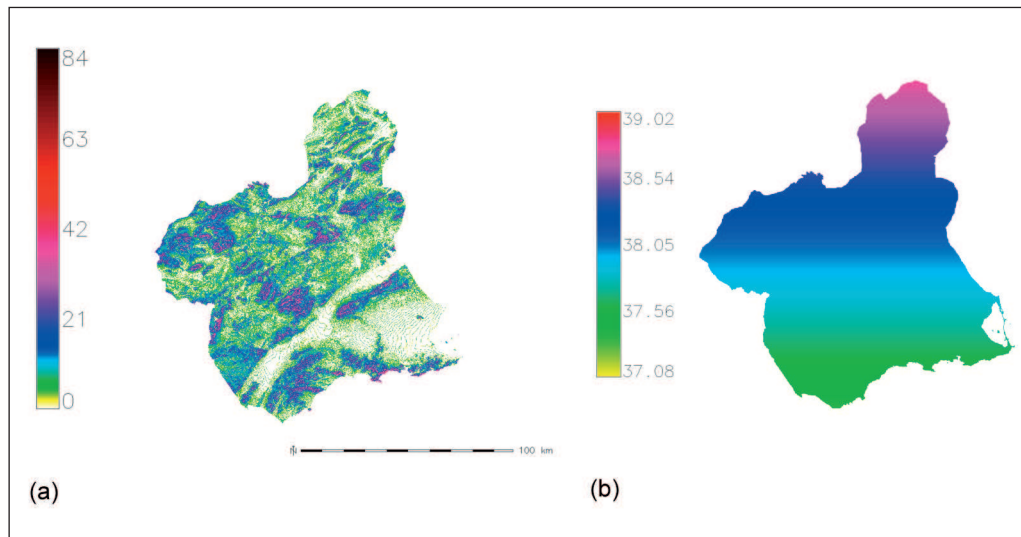


Fig. 9. Spatial distributions for the Region of Murcia: (a) slope, and (b) latitude.

- The *link turbidity* values, through SoDa Webpage (<http://www.helioclim.net>) were obtained at monthly scale for the 34 stations considered in the present study. The spatial distributions of monthly mean turbidity were obtained by interpolation.
- The *albedo* indicates the percentage of irradiation reflected depending on the surface. In this case, the spatial distribution of albedo was derived from MODIS MOD43B3 product.
- The *day* corresponds to Julian day of the year (1 to 365).

From the results of this command, the shortwave net radiation could be estimated from direct, diffuse and reflected radiation as follows,

$$R_N = R_{direct} - R_{diffuse} - R_{reflected} \quad (17)$$

2. Estimation of longwave net radiation

The longwave net radiation could be estimated by a balance between the radiation emitted by the sky and the reflected by earth's surface (Law of Stefan-Boltzmann), as follows,

$$R_L^\downarrow - R_L^\uparrow = \sigma \epsilon_a T_a^4 - \sigma \epsilon_s LST^4 \quad (18)$$

where $\sigma = 5.67 \cdot 10^{-8} \text{Wm}^{-2}\text{K}^{-4}$ is the constant of Stefan-Boltzmann, T_a (K), LST (K), ϵ_s is surface emissivity (or ϵ), and ϵ_a is the atmospheric emissivity estimated as,

$$\epsilon_a = \left[1 - (1 + \xi) \exp \left[- (1.2 + 3\xi)^{1/2} \right] \right] \quad \text{ó} \quad \epsilon_a = 0.56 + 0.259 \sqrt{e_a} \quad (19)$$

$$\xi = 46.5 \frac{e_a}{T_a} \quad (20)$$

where e_a is the air vapour pressure (kPa).

The heat flux from the soil G varies throughout the day, but its value is too small in comparison with R_N or λET . Therefore in the present work, the G value was not considered. However, the relation among R_N , NDVI, and G could be estimated by the equation from Moran *et al.* (1989).

$$G = 0.583 \exp \left[(-2.13 NDVI) R_N \right] \approx 0 \quad (21)$$

Therefore, the actual evapotranspiration ($\text{Wm}^{-2}\text{day}^{-1}$) will be,

$$\lambda ET = \phi \frac{\Delta}{\Delta + \gamma} (R_N - G) \quad (22)$$

And for the result expressed in mm/day, it is necessary to divide eq. (9) by 3047.6 factor. A schema of the developed methodology is presented in Fig. 10, and an example of spatial distributions of R_N and ET_{act} for the 24/07/09, are presented in Fig. 11.

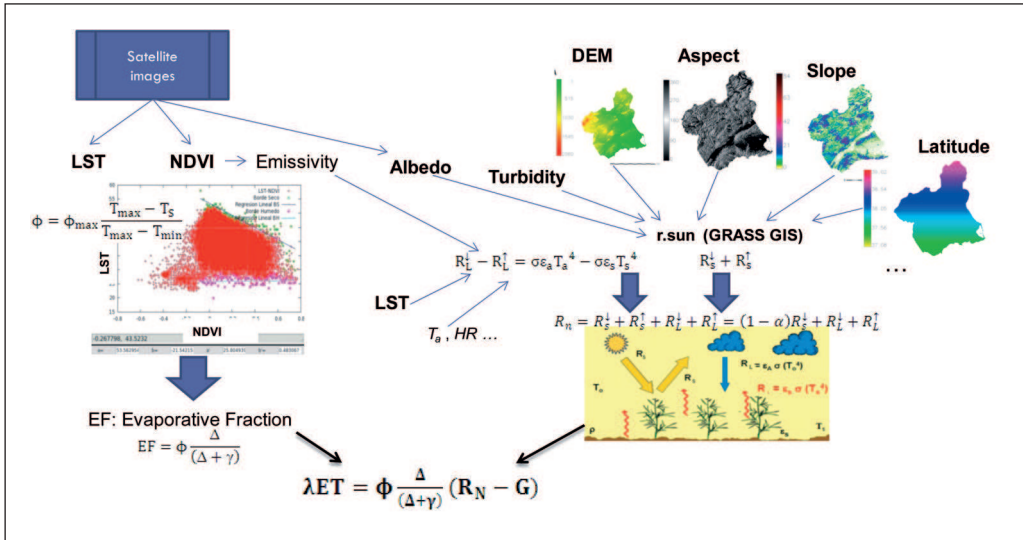


Fig. 10. Schema of the developed methodology.

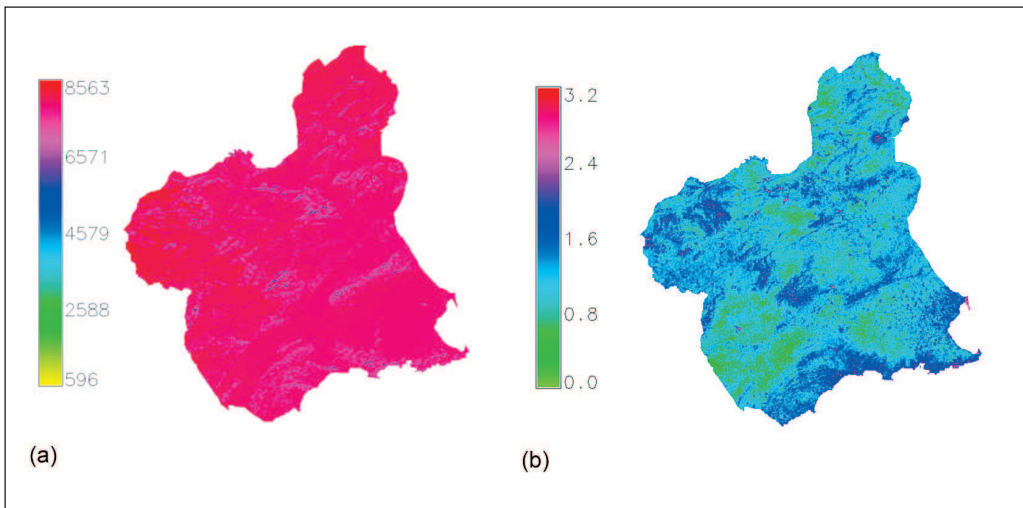


Fig. 11. Spatial distributions for the Region of Murcia: (a) R_N net radiation ($Wm^{-2}day^{-1}$), and (b) ET_{act} (mm/day).

VI – Conclusions

Climate change and variability predict a plausible negative scenario for the frequency and severity of drought events over the Segura River Basin (Garcia Galiano *et al.*, 2011). This situation endangers the continuity of significant irrigated areas in the Region of Murcia, which are important for the Region's economy. The monitoring of irrigated areas from remote sensing and direct estimation of actual evapotranspiration constitute valuable information for farmers. The method-

ology presented for estimating ET_{act} has been incorporated to GIS environment. Subsequently, the incorporation of the DEM and the derived topographical attributes have improved the spatial distributions of radiation estimates. These types of solutions are affordable from an operational point of view, for making recommendations of irrigation practices and schedules for farmers.

Acknowledgments

The funding from EU Project TELERIEG (Programme SUDOE INTERREG IV B), as well as the support from Project CGL2008-02530/BTE financed by the State Secretary of Research of Spanish Ministry of Science and Innovation (MICINN), are acknowledged.

References

- Gao B.-C. and Kaufman Y.J., 1998. *The MODIS Near-IR Water Vapor Algorithm. Algorithm Technical Background Document. Product ID: MOD05 - Total Precipitable Water.* p. 1-23. On line http://modis-atmos.gsfc.nasa.gov/_docs/atbd_mod03.pdf
- García Galiano S.G., Giraldo Osorio J.D., Urrea Mallebrera M., Mérida Abril A. and Tetay Botía C., 2011. Assessing drought hazard under non-stationary conditions on South East of Spain. In: *Risk in Water Resources Management*. (Eds. G. Blöschl, K. Takeuchi, S. Jain, A. Farnleitner, A. Schumann). IAHS Publ. 347, IAHS Press, CEH Wallingford, Oxfordshire, United Kingdom, p. 85-91.
- Giraut M., Minotti P. and Ludueña S., 2000. Integración de imágenes SAC-C, LANDSAT, y SPOT pancromático para la determinación de susceptibilidad hídrica. In: *IX Simposio Latinoamericano de Percepción Remota*, p. 1-8. On line http://www.hidricosargentina.gov.ar/selper_bol_giraut.pdf
- Grass, 2011. GRASS (Geographic Resources Analysis Support System) GIS 6.4.2svn Reference Manual. On line http://grass.osgeo.org/grass64/manuals/html64_user/index.html
- Jiang L. and Islam S. 2001. Estimation of surface evaporation map over southern Great Plains using remote sensing data. In: *Water Resources Research*, 37(2), p. 329-340.
- Jiang L., Islam S. and Carlson T.N., 2004. Uncertainties in latent heat flux measurements and estimation: implications for using a simplified approach with remote sensing data. In: *Can. J. Remote Sensing*, 30, p. 769-787.
- Jiménez-Muñoz J.C. and Sobrino J.A., 2003. A generalized single-channel method for retrieving land surface temperature from remote sensing data. In: *Journal of Geophysical Research*, 108, 1.
- Landsat Project Science Office 2002. Landsat 7 Science Data User's Handbook. Goddard Space Flight Center, Greenbelt, M.D.
- Remund J., Wald L., Lefevre M., Ranchin T. and Page J., 2003. Worldwide Linke turbidity information. Proceedings of ISES Solar World Congress, 16-19 June 2003, Göteborg, Sweden). CD-ROM published by International Solar Energy Society. On line: http://hal.archives-ouvertes.fr/docs/00/46/57/91/PDF/ises2003_linke.pdf
- Sandholt I., Rasmussen K. and Andersen J., 2002. A simple interpretation of the surface temperature/vegetation index space for assessment of surface moisture status. In: *Remote Sensing of Environment*, 79 (2-3), p. 213-224.
- SRBDAP, 2007. *Segura River Basin Drought Action Plan*. Hydrographic Confederation of Segura River Basin (CHS), Ministry of Environment, Marine and Rural Affairs, Spain.
- Šúri M. and Hofierka J. 2004. A new GIS-based solar radiation model and its application to photovoltaic assessments. In: *Transactions in GIS*, 8(2), p. 175-190.
- Urrea Mallebrera M., Mérida Abril A. and García Galiano S.G., 2011. Segura River Basin: Spanish Pilot River Basin Regarding Water Scarcity and Droughts. In: *Agricultural Drought Indices. Proceedings of the WMO/UNISDR Expert Group Meeting on Agricultural Drought Indices*. S. Mannava V.K., R.P. Motha, D.A. Wilhite and D.A. Wood (eds.), 2-4 June 2010, Murcia, Spain; Geneva, Switzerland: World Meteorological Organization. AGM-11, WMO/TD No. 1572; WAOB-2011. 219 p. 2-12.
- Valor E. and Caselles V., 1996. Mapping land surface emissivity from NDVI: Application to European, African, and South American Areas. In: *Remote Sensing of Environment*, 57 (3), p. 167-184.
- Voogt J.A. and Oke T.R., 2003. Thermal remote sensing of urban climates. In: *Remote Sensing of Environment*, 86 (3), p. 370-384.
- Zhang J., Wang Y. and Li Y., 2006. A C++ program for retrieving land surface temperature from the data of Landsat TM/ETM+ band 6. In: *Computers & Geosciences*, 32, p. 1796-1805.